



Tsiavos, A., Sextos, A., Stavridis, A., Dietz, M., Dihoru, L., & Alexander, N. A. (2020). Large-scale experimental investigation of a low-cost PVC 'sand-wich' (PVC-s) seismic isolation for developing countries. *Earthquake Spectra*.  
<https://doi.org/10.1177/8755293020935149>

Peer reviewed version

Link to published version (if available):  
[10.1177/8755293020935149](https://doi.org/10.1177/8755293020935149)

[Link to publication record in Explore Bristol Research](#)  
PDF-document

This is the author accepted manuscript (AAM). The final published version (version of record) is available online via SAGE Publications at <https://journals.sagepub.com/doi/abs/10.1177/8755293020935149> . Please refer to any applicable terms of use of the publisher.

## University of Bristol - Explore Bristol Research

### General rights

This document is made available in accordance with publisher policies. Please cite only the published version using the reference above. Full terms of use are available:  
<http://www.bristol.ac.uk/red/research-policy/pure/user-guides/ebr-terms/>

# Large-scale experimental investigation of a low-cost PVC ‘sand-wich’ (PVC-s) seismic isolation for developing countries

Anastasios Tsiavos,<sup>a)</sup> M.EERI, Anastasios Sextos,<sup>a)</sup> M.EERI,  
Andreas Stavridis,<sup>b)</sup> M.EERI, Matt Dietz,<sup>a)</sup> Luiza Dihoru,<sup>a)</sup>  
and Nicholas A. Alexander,<sup>a)</sup>

This study presents a large-scale experimental investigation on the seismic performance of an innovative, low-cost seismic isolation system for developing countries. It is based on the beneficial effect of the encapsulation of sand grains between two PVC surfaces on the initiation of sliding and the dissipation of seismic energy between the surfaces. A three-times scaled down, idealized, seismically isolated model of a prototype single-story structure located in Nepal is subjected to an ensemble of recorded earthquake ground motion excitations. The experimentally derived response of the seismically isolated structure is compared with the response of the corresponding fixed-base structure. This system is part of a wider hybrid design approach where the structure is designed to resist the seismic forces at the design acceleration level. The seismic isolation system sets an upper bound to the response of the structure for ground motion excitations exceeding the design level.

## INTRODUCTION

The determination of economical and resource-effective engineering solutions for the protection of our communities from seismic hazard is of paramount importance to the safety and the sustainable growth of our communities. A wide spectrum of highly engineered seismic isolation techniques that focus on the modification of the response of buildings and bridges to earthquake ground motion excitation has been developed during the last four decades to increase the seismic safety of these structures (Kelly 1990, Buckle and Mayes 1990, Constantinou et al. 1992, Heaton et al. 1995, Naeim and Kelly 1999, Naeim 2019). The fundamental parameters that influence the frictional properties of the existing highly

---

<sup>a)</sup> Department of Civil Engineering, University of Bristol, Bristol, United Kingdom

<sup>b)</sup> Department of Civil, Structural and Environmental Engineering, University at Buffalo, Buffalo, NY 14260, United States

engineered sliding seismic isolation techniques have been quantified by Kumar et al. (2015), Furinghetti et al. (2019a) and Quaglini et al. (2019).

Notwithstanding the significant contribution of these seismic isolation systems to the reduction of earthquake-induced structural damage and losses, the unambiguously high installation cost and the resource-demanding construction process inhibit their application to countries with limited material and financial resources (Kelly 2002, Yang et al. 2010).

In view of these limitations, several researchers have investigated the sliding and rolling frictional resistance of a broad variety of low-shear-strength material interfaces to facilitate the design of low-cost seismic isolation strategies based on the premise of a sliding energy dissipation mechanism. In the beginning of the 20<sup>th</sup> century, Calanterioris (1909) proposed the design of a building founded on a layer of talc as a low-cost sliding seismic isolation system. A similar seismic isolation system, consisting of a layer of soil and a layer of soft mud was adopted by Wright (1977), who engineered the seismically isolated Imperial hotel in Tokyo. The application of low-cost sliding isolation systems to masonry structures was experimentally investigated by Li et al. (1989) and Nanda et al. (2016), who performed shaking table tests on the sliding response of a masonry structure based on different sliding interfaces. Jampole et al. (2016) conducted full-scale shaking table tests towards the implementation of a sliding seismic isolation system in low-rise lightweight residential buildings. The seismic behavior of lightweight structures seismically isolated with a system consisting of high-strength concrete slabs and a deformable steel rolling ball was investigated by Cilsalar and Constantinou (2019).

However, the challenge of the seismic protection of structures in developing countries for a wide variety of earthquake motion intensities remains a complex task that necessitates the consideration of a combination of seismic mitigation mechanisms, each being activated at a different ground motion acceleration level. Following the above line of thought, this study focuses on a hybrid design approach, combining two seismic mitigation mechanisms: The structure withstands seismic forces as normal up to the design acceleration and once this is exceeded, a sliding seismic isolation system acts as a fuse which effectively sets an upper bound to the forces that can be transferred to the building. This hybrid design approach was proposed by Tsiavos et al. (2019) investigating experimentally at small-scale the static and dynamic sliding response of a structure founded on a sand-rubber layer as a seismic isolation system for developing countries. The large-scale investigation of this seismic isolation system has led to significant rocking response, before the sliding response of the structure was triggered. Within this context, the determination of a seismic isolation system that facilitates

the activation of sliding at a relatively low acceleration threshold is critical for the economical design of a structure and the efficiency of the proposed hybrid design approach.

The mechanics of rolling-sliding behavior of structures can emerge as a natural means of decreasing the abovementioned sliding acceleration threshold, whose potential has still not been clearly established.

The quantification of the fundamental laws that govern the sliding and rolling frictional resistance between two contact interfaces dates back to several centuries ago. Coulomb (1785) stated that the friction of a rolling wheel is analogous to the vertical force acting on the wheel, and inversely proportional to the radius of the wheel. Dupuit (1842) incorporated the material deformability in the determination of the rolling friction by suggesting that the material subjected to a rolling motion of an object exhibits plastic deformation after rolling occurs. Bowden and Tabor (1956) attributed the sliding frictional resistance between two solid surfaces to two types of forces: first, an adhesion force that is inextricably linked to the shear strength of the interface between the two surfaces and the contact area between microscopically rough surface irregularities, defined as asperities. Second, a plastic deformation (plowing) force highly correlated with the relative hardness of the materials in contact and the uniformity of the grains of these materials (Shooter and Tabor 1952).

The aforementioned plowing component of friction can be significantly decreased by the encapsulation of sand particles between two hard surfaces in a ‘sand-wich’ configuration. O’Rourke et al. (1990) showed that the increase of the hardness of a polymer surface reduces substantially the friction of its interface against sand particles and suggested the manifestation of a rolling behavior accounting for the friction of sand particles against smooth polymer interfaces. Dove and Frost (1999) concluded that the interface of spherical, uniform particles against hard polymer (PolyVinyl Chloride-PVC) surfaces exhibits initiation of sliding at a significantly lower friction level compared to the case of angular, non-uniform particles. Ebrahimian et al. (2019) presented a numerical investigation on the interface shearing behavior of a thin granular soil layer, encapsulated by two rigid surfaces of different roughness.

The sliding seismic isolation system proposed in this study capitalizes on the presented low frictional resistance of sand particles against polymers. The PVC-sand-wich (PVC-s) seismic isolation is based on the inclusion (sandwiching) of a thin film of sand grains between two PVC sheets. This seismic isolation strategy belongs to the family of geotechnical seismic isolation (GSI) strategies, as defined by Tsang and Pitilakis (2019). The large-scale shaking table tests presented in this study show that the seismic isolation of a low-rise structure based



on this novel PVC-s sliding isolation system leads to an attractively low sliding acceleration threshold in the range of 0.25-0.3g.

Along these lines, the main goal of this study is to investigate means of low-cost enhancement of structural performance and in particular a hybrid design, which includes the seismic resistance of the structure at the design level and the activation of the PVC-s seismic isolation for the above-design earthquake intensities. In a realistic case the friction coefficient and several other parameters of the proposed seismic isolation system cannot be controlled but this is not a major issue given that PVC-s can only have a beneficial effect on the seismic response of the structure. The application of the presented hybrid design approach to masonry structures can be combined with standard strengthening of masonry walls using wire mesh as well as with the installation of a light roof on the structure that reduces its total mass.

The PVC-s is the seismic isolation system that has been experimentally qualified in this study as a key component that facilitates the implementation of the presented hybrid design approach due to its attractive frictional characteristics and the initiation of sliding at a low acceleration threshold close to 0.25-0.3g. The comparison of the experimentally observed response of the seismically isolated structure to an ensemble of ground motion excitations with the experimentally derived fixed-base response illuminates the engineering merit of this seismic isolation system towards the reduction of the seismic forces and the seismic damage of low-rise structures in developing countries.

## ISOLATION CONCEPT FOR THE PROTOTYPE STRUCTURE

The prototype is a one-storey unreinforced masonry structure with a light steel roof supported by 23cm thick masonry walls. The hybrid design approach presented in this study shares the same light roof concept with the prototype structure as a means of increasing the seismic safety of the structure. This structure is a typical example of a masonry one-classroom school building located in Nepal. The light-roof concept is commonly met in Nepal after the destructive 2015 Gorkha earthquake in the construction of structures known as Temporary Learning Centers (TLCs), providing safe educational spaces for children. The dimensions of the school building are shown in Fig. 1. The vertical stress on the foundation due to the weight of the structure is  $\sigma'_v=9\text{kPa}$ .

Fig. 1 elucidates the design of the proposed innovative PVC-s seismic isolation system. The fundamental design configuration entails the encapsulation of sand grains between two hard 6mm thick PVC surfaces, positioned below the 20cm thick concrete foundation slab of the

structure. The encapsulation of sand grains of a predetermined mass facilitates a sliding behavior of the top PVC sheet against the bottom PVC sheet, enhanced by the low rolling resistance of the sand particles.

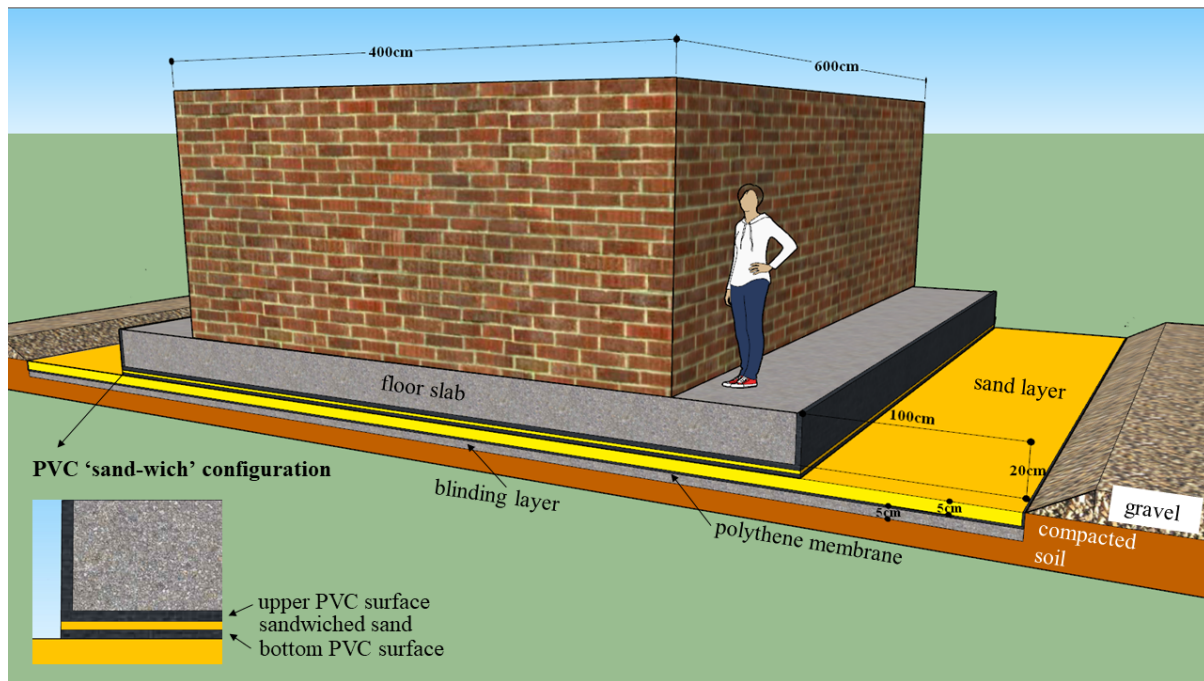


**Figure 1.** Masonry school prototype structure located in Nepal (Dimensions in cm).

The application of the PVC-s seismic isolation to the prototype structure entails the following steps: A 10cm deep excavation is performed first at the site of the structure. The lateral extent of the excavation is wider than that of the intended foundation slab by 100cm, thus minimizing the risk of pounding of the foundation slab against the surrounding soil due to an excessive sliding displacement of the structure. A 30° inclined, 10cm thick gravel layer based on the surrounding soil is used as a restraining mechanism to ameliorate the consequences due to a potential exceedance of the maximum expected sliding displacement estimates.

A 5cm thick sand layer is enclosed at its bottom and lateral sides by a polythene membrane sheet and based on a 5cm thick sub-foundation blinding layer, aimed at the formation of a levelled, stiff base below the seismically isolated structural system. The unreinforced blinding layer is founded on the existing soil at the site of the structure below the 10cm deep excavation level, which should be compacted before the concrete casting of the blinding layer.

The bottom PVC surface of the proposed isolation system is placed on the 5cm thick sand layer. A thin film of sand particles is placed above the bottom PVC layer and below the upper

PVC layer, thus creating the intended ‘sand-wich’ configuration (Fig. 1). The 20cm thick concrete slab is casted on the upper PVC surface, which remains positioned below the foundation slab as an undegradable, permanent formwork. The masonry structure is constructed on the concrete slab, after it hardens.

The low cost of the presented PVC-s seismic isolation comparing to the existing highly engineered isolation systems emerges from the minimization of the construction and transportation cost of the isolation system through its simple construction based on materials that are locally available in developing countries, such as PVC and sand. Furthermore, the presented floor slab-blinking layer configuration leads to a substantially lower construction cost compared to the existing highly engineered seismic isolation systems, requiring the construction of two reinforced concrete slabs: One slab creating a diaphragm above the isolation devices and one foundation slab below the level of these devices. However, the slab configuration of the proposed low-cost isolation system shown in Fig. 1 comprises the construction of only one reinforced concrete floor slab above the isolation system and a 5cm thick unreinforced blinding concrete layer below the isolation system. Moreover, the ease of the application of the presented seismic isolation, which does not necessitate a project specific testing of the isolation system, facilitates an additional cost reduction and higher applicability to a developing country compared to the existing seismic isolation systems.

## EXPERIMENTAL SETUP

A three-times-scaled down model of the aforementioned masonry prototype structure is designed as shown in Fig. 2. The test structure is made out of steel due to the low vulnerability and the transportability of the structure convenient for a parametric investigation and it is designed to meet three design objectives: First, the height of the steel model is chosen to correspond to 2/3 of the height of the scaled-down height of the masonry walls of the prototype (83cm), thus maintaining the acting point of the equivalent seismic force between the scaled-down steel frame and its masonry counterpart. Second, the model structure is designed to have the same fixed-base vibration period  $T_x=0.085s$  (frequency  $f_x=12Hz$ ) in X-Direction of shaking (Fig. 2) with the period of the prototype structure, calculated using the stiffness estimation for unreinforced masonry walls proposed by Wilding and Beyer (2018). Third, the sand layer below the model structure is subjected to the same vertical foundation stress level  $\sigma'_v=9kPa$  as the prototype structure.

The investigated structure is a 1t steel structure and it is based on a 20cm thick, 1.3t reinforced concrete slab. The concrete slab is founded on a 5cm thick sand layer, deposited with zero-height drop. The density of the sand layer is  $1540\text{kg/m}^3$ . The abovementioned ratio is defined in this study as sand surface density ( $\text{g/m}^2$ ). The properties of the Leighton Buzzard 14-25 sand used in this study are summarized in Table 1.

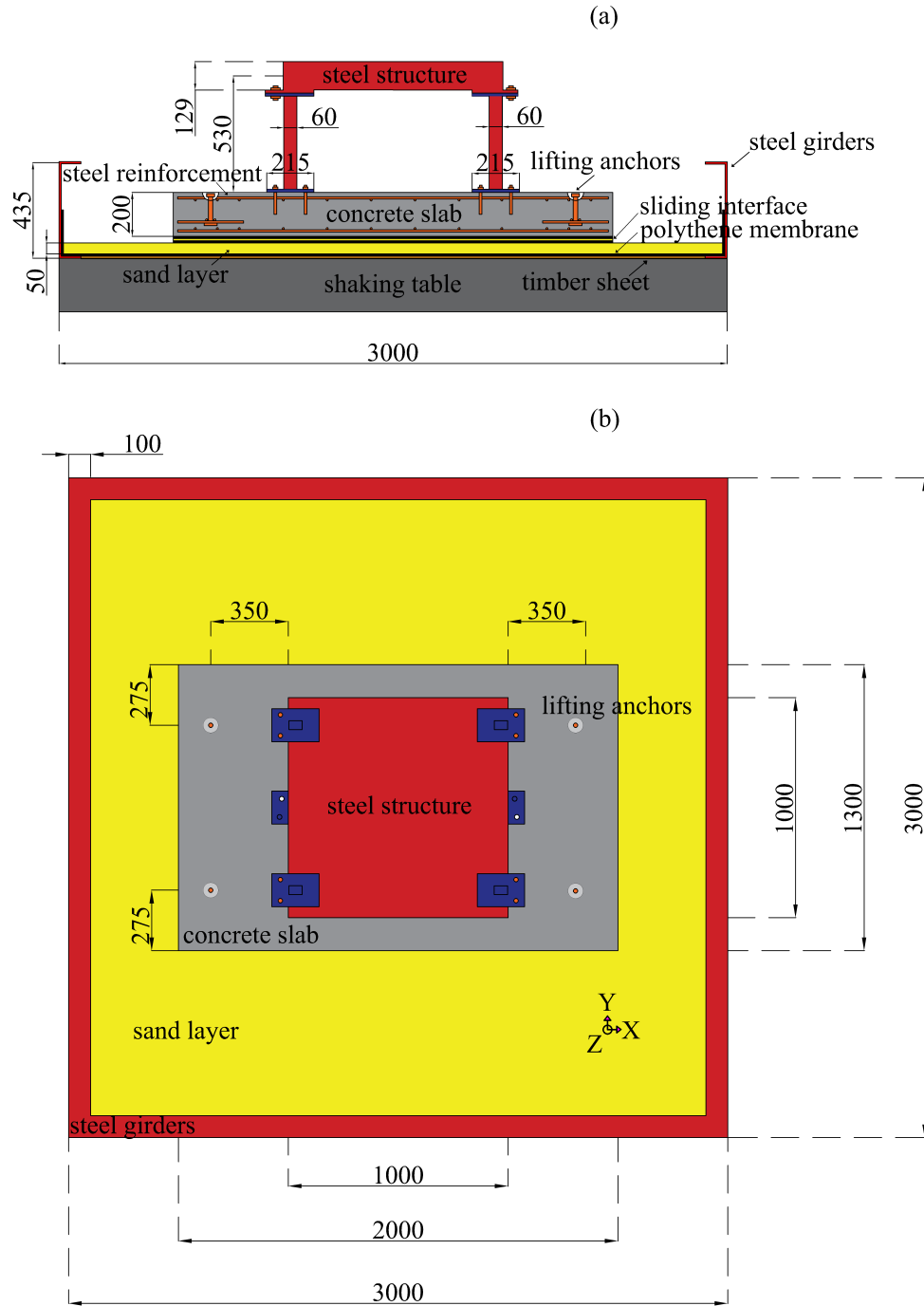


**Figure 2.** (a) Cross-section and (b) plan view of the design of the experimental setup (Dimensions in mm).

**Table 1.** Characteristics of the Leighton Buzzard 14-25 sand used in this study.

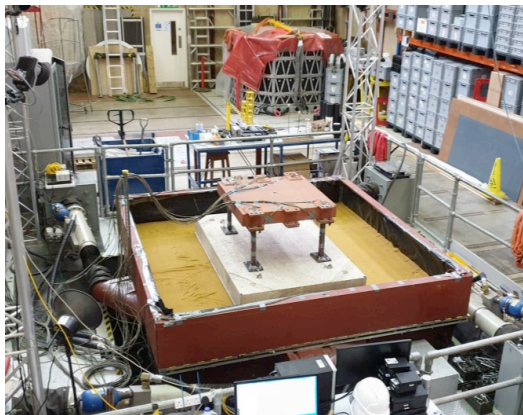
Specific gravity $G_s$	Void ratio $e_{max}$	Void ratio $e_{min}$	Mean size $D_{50}$ (mm)	$C_u=D_{60}/D_{10}$	$C_g=D_{30}^2/D_{60}D_{10}$
2.65	0.84	0.53	0.883	1.439	0.996

The seismic response of this structure is assessed based on experimental large-scale testing at the 3mx3m shaking table of University of Bristol. The shaking table has a six-degree-of-freedom motion testing capability. The maximum payload of the table is 15t. Depending on the loading, the shaking table can apply acceleration amplitudes up to 5g.

Four C-shaped steel girders are fixed on the edges of the shaking table of University of Bristol to enclose the sand layer and prevent the structure from excessive sliding displacements. A polythene membrane is placed around and below the sand layer to inhibit any leakage of sand grains. A timber sheet is attached above the shaking table and below the polythene membrane to act as a secondary protection mechanism from leakage of sand in case of damage in the polythene membrane.

## INSTRUMENTATION

The constructed experimental setup and the applied instrumentation are shown in Fig. 3. The instrumentation of the experimental setup shown in Fig. 4 consists of 25 accelerometers and 16 infrared displacement markers, which are tracked by 5 infrared high-speed cameras. The cameras are fixed on a rigid aluminium frame, 3m above the shaking table. Each accelerometer (red colour) measures the acceleration in one direction, while each marker (yellow colour) tracks the displacement in three directions at selected locations of interest. All measurements are synchronized.



(a)



(b)

**Figure 3.** (a) Overview and (b) side view of the constructed experimental setup.

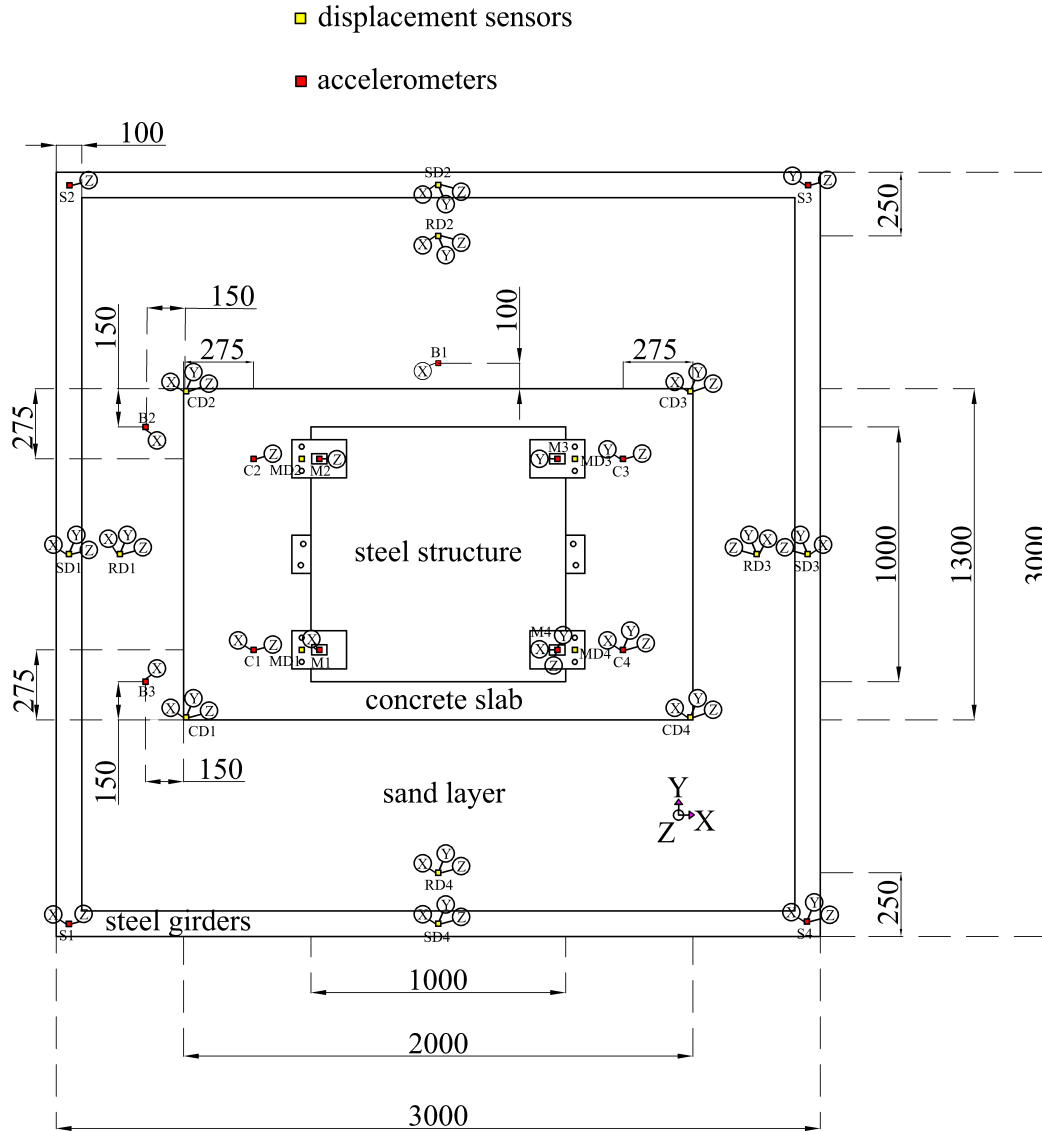


**Figure 4.** Instrumentation plan of the experimental setup (Dimensions in mm).

#### INSTALLATION OF PVC SURFACES AND DEPOSITION OF SAND

The PVC sliding surfaces were installed parallel to each other and the sand foundation layer, thus not considering possible inclinations, which could be unintentionally formed during the application of the proposed system in the field. However, Furinghetti et al. (2019b) suggest that the consideration of these inclinations leads to low variation of the fundamental response parameters (displacement, base shear).

The deposition of sand between the two PVC sheets is performed as shown in Fig. 5. The use of a 2.2mm sieve facilitated the uniform distribution of the sand along the bottom PVC surface, thus allowing a uniform encapsulation of the sandwiched sand between the two PVC sheets.



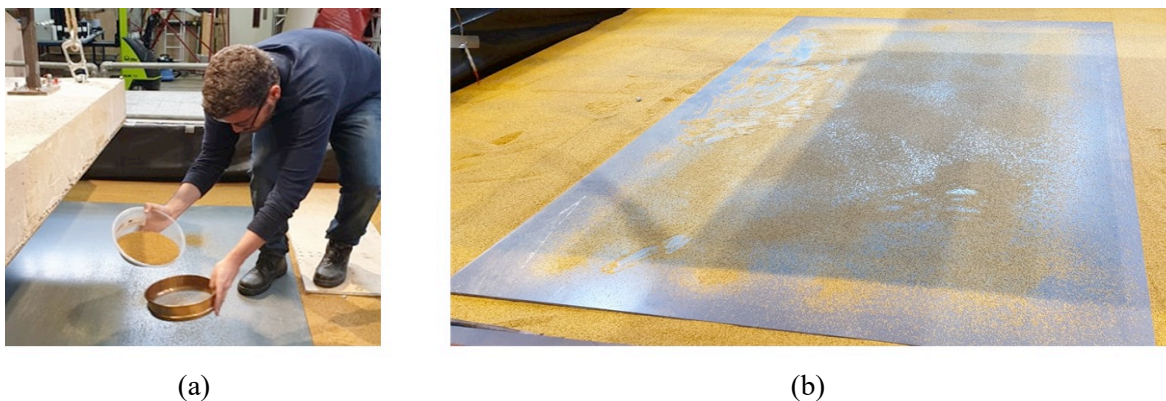


**Figure 5.** (a) Deposition of sandwiched sand and (b) bottom PVC surface after sand deposition.

## TESTING PROTOCOL

A white-noise test with amplitude  $A=0.05g$  and frequency range  $f=0-100\text{Hz}$  is performed for all experimental configurations presented in this study for the determination of the fundamental frequencies of the structural system. A spectrum analysis is employed to compute the Frequency Response Function (FRF) between the measured acceleration input and the measured acceleration output on the top of the steel slab of the structure (M1 in Fig. 4). The peaks of the FRF correspond to the modal frequencies. The experimentally derived, flexible-base fundamental vibration period of the presented structural system (Fig. 2-4) in X-Direction is  $\tilde{T}_x=0.09\text{s}$  ( $\tilde{f}_x=11\text{Hz}$ ). The small thickness of the bottom sand layer (5cm) is chosen to minimize the rocking response of the structure due to potential soil-structure-interaction effects. Accordingly, the measured period lengthening  $\tilde{T}_x/T_x=1.05$  due to soil-structure-interaction with respect to the fixed-base period value  $T_x$  lies in the low period-lengthening range of the values presented by Stewart and Fenves (1998), Mylonakis and Gazetas (2000), Taciroglu et al. (2016) and Star et al. (2019) for a wide range of structural systems.

The structure is subjected to nine strong earthquake ground motion excitations of different frequency content, obtained from the PEER NGA Database (2018) and the USGS Center for Engineering Strong Motion Data (2018). The horizontal components of the selected ground motion records 1-8 shown in Table 2 are scaled to two peak ground acceleration (PGA) levels: 0.4g and 0.6g and applied in X-Direction (Fig. 2, 4). The horizontal components of L'Aquila 2009 ground motion record (No. 9) are scaled to a peak ground acceleration (PGA) level of 0.5g. The three components (two horizontal and one vertical) of this record are applied simultaneously in directions X, Y and Z (Fig. 2, 4). The acceleration response spectra of the ground motion records considered in this study, scaled at a PGA=0.4g, are shown in Fig. 6.

**Table 2.** Testing protocol of real earthquake records used in this study (PEER NGA Database, 2018 and USGS Center for Engineering Strong Motion Data, 2018).

No.	Date	Earthquake and Site	$M_w$	$R$ (km)	Component	Scaled PGA (g)
1	21/9/1999	Chi-Chi, CHY080	7.6	2.69	CHY080-E	0.4
2	21/9/1999	Chi-Chi, CHY080	7.6	2.69	CHY080-E	0.6
3	25/4/2015	Gorkha, KTP	7.8	75.8	KTP-NS	0.4
4	25/4/2015	Gorkha, KTP	7.8	75.8	KTP-NS	0.6
5	6/4/2009	L'Aquila, Parking	6.3	5.38	LAQ-AM043XTE	0.4
6	6/4/2009	L'Aquila, Parking	6.3	5.38	LAQ-AM043XTE	0.6
7	17/1/1995	Kobe, Nishi-Akashi	6.9	7.08	KOBE_NIS000	0.4
8	17/1/1995	Kobe, Nishi-Akashi	6.9	7.08	KOBE_NIS000	0.6
9	6/4/2009	L'Aquila, Parking	6.3	5.38	LAQ-AM043XTE LAQ-AM043YLN LAQ-AM043ZUP	0.5

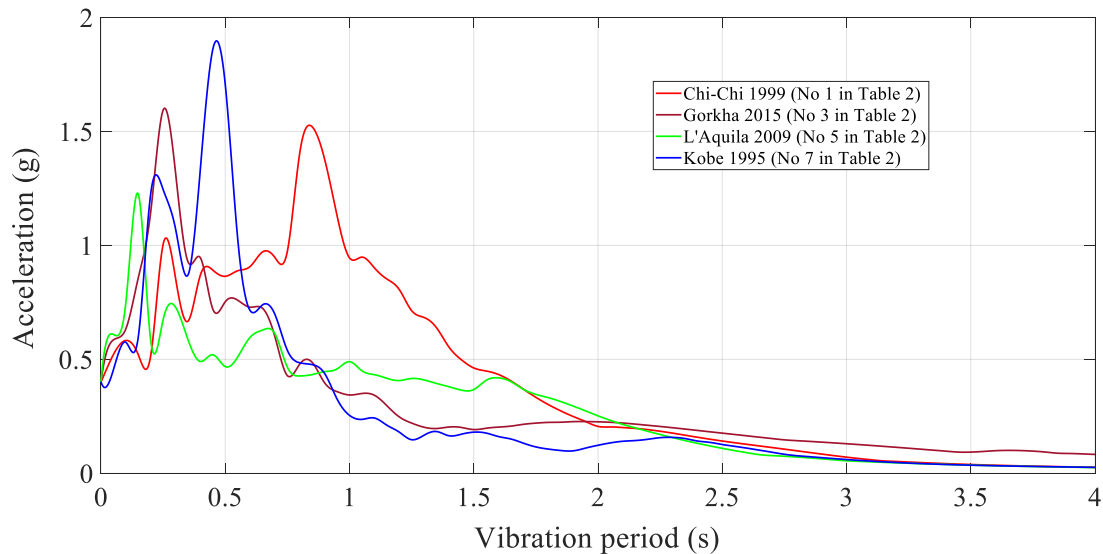


**Figure 6.** Acceleration response spectra of the ground motion records used in this study, scaled at a PGA=0.4g.

## DIMENSIONAL ANALYSIS

The maintenance of the similitude between the sliding behavior of the model structure and the prototype is fulfilled through the preservation of two dimensionless ratios  $\Pi_1$ ,  $\Pi_2$ . The dimensionless strength ratio  $\Pi_1 = \mu g / \text{PGA}$  ( $\mu$  being the static friction coefficient and  $g$  the acceleration of gravity) expresses the strength of the sliding interface relative to the ground motion intensity. The vibration period ratio  $\Pi_2 = \tilde{T}_x / T_g$  represents the relation between the flexible-base period  $\tilde{T}_x$  of the structural system over the predominant period of the excitation



$T_g$ , defined as the period where the 5% velocity spectrum attains its maximum (Miranda and Bertero 1994, Mylonakis and Gazetas 2000).

The friction coefficient  $\mu$  of an interface between a polymer surface and a granular material (Dove and Frost 1999) varies for different vertical stress levels. To avoid further complications, the sandwiched sand grains and the sand layer below the foundation of the model structure are subjected to the same vertical stress level  $\sigma'_v=9\text{kPa}$  as the foundation stress level below the prototype structure. Therefore, the friction coefficient and the associated dimensionless strength ratio are preserved between the model and the prototype structure, thus maintaining the similitude in the sliding behavior of the two structures. The model structure is designed to have the same elastic fixed-base vibration period  $T_x=0.085\text{s}$  with the prototype structure. The measured flexible-base vibration period value of the structure  $\tilde{T}_x$  is very close to the corresponding fixed-base value  $T_x$ . Thus, the frequency characteristics of the applied ground motions remain unchanged with respect to the original earthquake ground motion records and the ratio  $\tilde{T}_x/T_g$  is maintained between the model and the prototype structure.

## EXPERIMENTAL INVESTIGATION

### SLIDING BEHAVIOR OF PVC-S SEISMIC ISOLATION

The hybrid design approach presented in this study has explored different seismic isolation systems as a means of seismic protection mechanisms, focusing on minimizing the ground motion acceleration threshold after which sliding occurs. The large-scale investigation of the seismic isolation of the structure presented in Fig. 2 using a sand-rubber layer (Tsiavos et al. 2019) of thickness varying from 5cm-20cm has led to significant rocking response before the manifestation of the sliding behavior. Hence, the exploration of a seismic isolation system consisting of a granular layer with a minimum thickness of 5cm emerged as a necessity derived from the intended increase of vertical stiffness below the sliding interface of the structure. The choice of the PVC-s as a sliding seismic isolation system and the design configuration shown in Fig. 2 are an outcome of an iteratively determined balance between the attractive experimentally derived frictional properties of sand against polymers (O'Rourke et al. 1990, Dove and Frost 1999) and the desirable increase of vertical stiffness below the foundation slab of the structure.

The favorable role of the encapsulation of sand between the two PVC sheets and the sequence of the activation of the two inherent energy dissipation mechanisms, incorporated in

the design of the proposed seismic isolation system are illustrated in Fig. 7, 8: The presence of uniformly distributed 2000g of sandwiched sand (surface density  $750\text{g/m}^2$  with respect to the bottom PVC surface) triggers the initiation of sliding of the upper PVC sheet against the bottom PVC sheet of the model structure subjected to Chi-Chi 1999 ground motion excitation (No. 1 in Table 2).

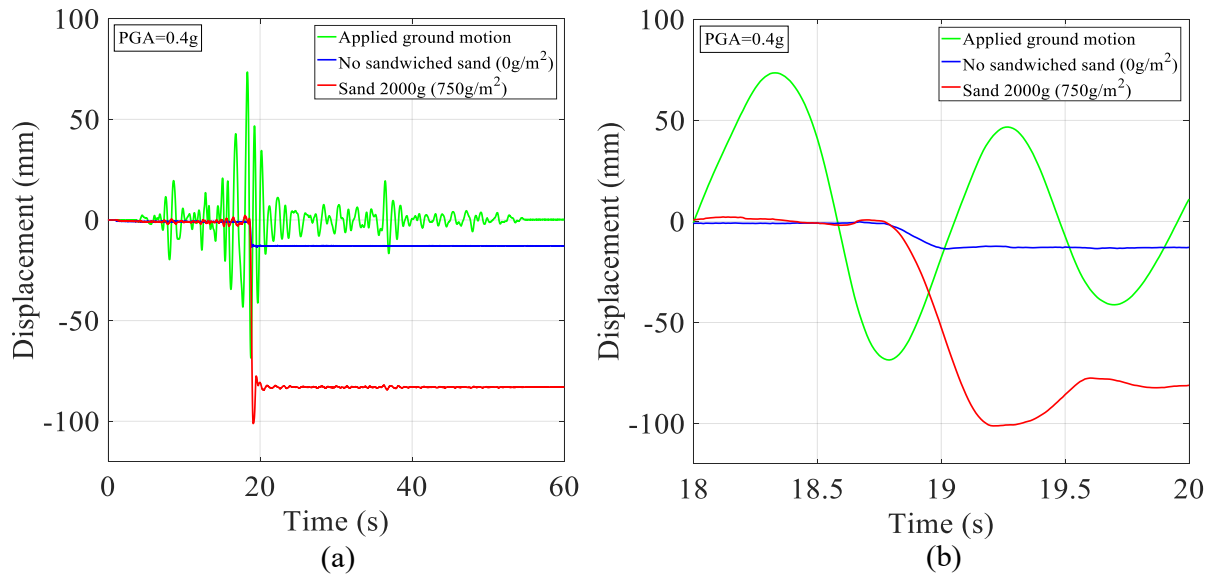


**Figure 7.** (a) Full and (b) magnified sliding displacement time history response of the concrete slab relative to the shaking table motion (mean value of CDX-SDX in Fig. 4) subjected to Chi-Chi 1999 ground motion record (No. 1 in Table 2) for two different sand configurations between the two PVC sheets.

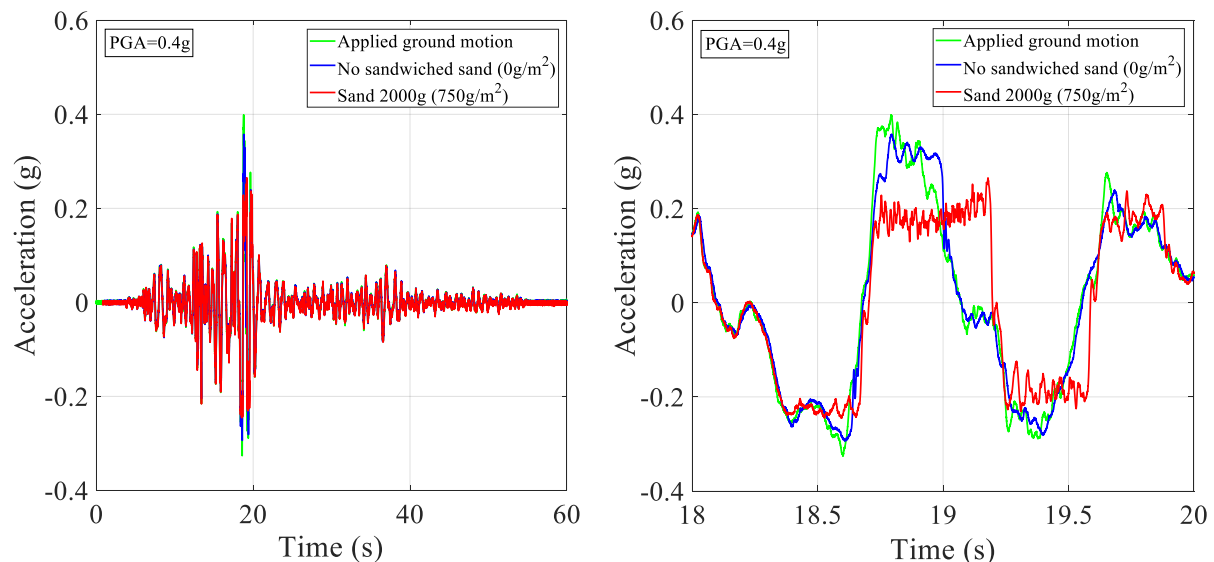


**Figure 8.** (a) Full and (b) magnified acceleration time history response of the concrete slab (mean value of C1X and C4X in Fig. 4) subjected to Chi-Chi 1999 ground motion record (No. 1 in Table 2) for two different sand configurations between the two PVC sheets.

This sliding behavior expressed by a maximum displacement of 10cm (Fig. 7) is attributed to the exceedance of the rolling frictional resistance of the sand grains and leads to a maximum acceleration response of 0.25g (Fig. 8) at the level of the concrete slab (C1X, C4X in Fig. 4). This maximum acceleration response indicates the value of the friction coefficient of the interface  $\mu=0.25$  and is significantly lower than the corresponding acceleration response value of 0.35g, observed for the case in which the presented seismic isolation system does not include any sand between the two PVC sheets (Fig. 8). In this case, there is no relative displacement between the two PVC sheets, which exhibit a sliding behavior expressed by a maximum displacement of 1.3cm against the 5cm thick sand sub-foundation layer (Fig. 7).

The first sliding mechanism of the presented isolation system is activated between the two PVC sheets at a  $PGA=0.25g$ . The secondary sliding mechanism is activated, in case of no sandwiched sand enclosure, between the bottom PVC sheet and the sand sub-foundation layer at a  $PGA=0.35g$ . The existence of two sliding mechanisms illuminates the redundancy and the robustness of the presented dual seismic isolation system.

A parametric investigation of the acceleration response of the test structure subjected to Chi-Chi 1999 ground motion excitation (No. 1 in Table 2) for varying sand surface density values is performed. The experimentally derived results of this investigation are shown in Table 3 and Fig. 9. Two sliding events (first sliding event:  $18.7s \leq t \leq 19.2s$ , second sliding event:  $19.2s \leq t \leq 19.6s$ ) were used for the statistical evaluation of the friction coefficient  $\mu$  during the excitation of the structure. The mean, standard deviation and 95% confidence interval values of the friction coefficient  $\mu$  derived from the sliding events magnified in Fig. 9b are also shown on Table 3. Evidently, there is a range of sand surface densities between 40 and 750g/m<sup>2</sup> that lead to comparable performance in the response of the seismically isolated structure, expressed by the lowest mean friction coefficient value. Among these values, the sand surface density value of 750g/m<sup>2</sup> is recommended in this study as the one yielding the lowest dispersion of the friction coefficient value, leading to the lowest 95th percentile (Table 3). The aforementioned optimal range of sand surface density values determined for this ground motion excitation is generalized through the excitation of the structure by the ground motions presented in Table 2.

As shown in Fig. 9 an increase of the sand surface density from 100g (40g/m<sup>2</sup>) to 2000g (750g/m<sup>2</sup>) reduces the maximum acceleration response and the standard deviation of the oscillations observed during the sliding phase of the upper PVC layer against the bottom PVC

layer. This reduction in the maximum of the acceleration response is consistent with the decrease of the corresponding 95th percentile value of the friction coefficient from 0.29 to 0.23 (Table 3), although the mean friction values for the two surface densities are comparable, namely 0.179 and 0.187. Nevertheless, a further increase of this amount from 2000g to 4000g (1500g/m<sup>2</sup>) is detrimental due to the increase of the maximum acceleration response and the associated friction coefficient to a 95th percentile value  $\mu=0.34$  and a mean value of  $\mu=0.3$ .

**Table 3.** Experimentally derived mean, standard deviation and 95% confidence interval values of friction coefficient  $\mu$  for varying sand surface density values.

PGA (g)	Sand surface density (g/m <sup>2</sup> )	Mean $\hat{\mu}$	Standard deviation $\sigma$	95% confidence interval ( $\hat{\mu} \pm 2\sigma$ )
0.4	0	0.285	0.015	$0.25 \leq \mu \leq 0.32$
0.4	40	0.179	0.056	$0.07 \leq \mu \leq 0.29$
0.4	750	0.187	0.024	$0.14 \leq \mu \leq 0.23$
0.4	1500	0.302	0.020	$0.26 \leq \mu \leq 0.34$

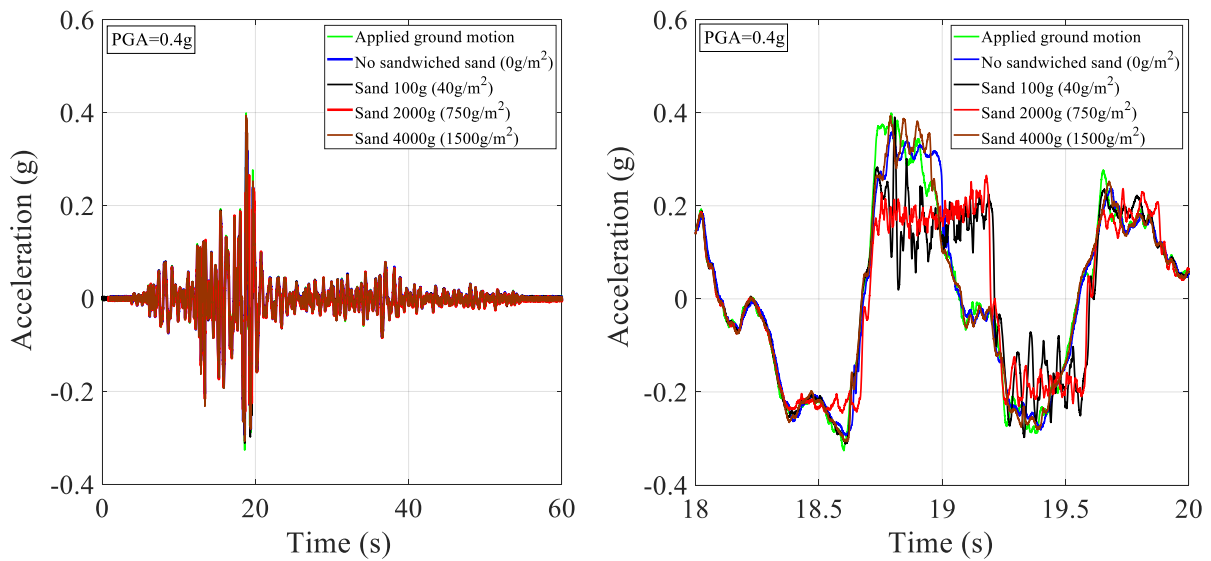


**Figure 9.** (a) Full and (b) magnified acceleration time history response of the concrete slab (mean value of C1X and C4X in Fig. 4) subjected to Chi-Chi 1999 ground motion record (No. 1 in Table 2) for varying amounts of sandwiched sand between the two PVC sheets.

The confirmation of the repeatability of the beneficial effect of the proposed seismic isolation system is an essential step towards the application of this seismic isolation strategy to structures in earthquake-prone areas. The investigation of the response of the structure for subsequent ground motions simulates the effect of aftershocks or successive earthquake events on the efficiency of the presented seismic isolation system when that is already activated and displaced. The sliding displacement and acceleration response of the model structure to three

subsequent Chi-Chi 1999 ground motion excitations of  $PGA=0.4g$  is shown in Fig. 10, 11, respectively.

As shown in Fig. 10, the maximum and the residual components of the sliding displacement of the model structure (relative to the shaking table) due to the applied subsequent ground motion excitations deviate roughly 20% from the corresponding values attributed to the first applied ground motion excitation.

Similar to the system developed by Jampole et al. (2016), the proposed seismic isolation system does not provide any recentering force, but instead relies on friction alone. The residual displacement obtained for this ground motion excitation corresponds to the maximum residual displacement amplitude obtained in this study, reaching roughly 5% of the concrete slab width, namely 10cm. However, the presence of potential excessive sliding displacements is explicitly accounted in the design of the prototype structure by the wide extent of the excavation and the presence of additional space (margin) surrounding the foundation slab of the structure. Furthermore, the recentering of the presented one-storey prototype structure, displaced at maximum by 10cm from the original configuration after the earthquake event could be performed via a pulling force created by a truck. Hence, the risk of pounding due to these displacements is minimized. Future investigations could more precisely determine the required displacement safety margin for the prevention of this pounding. This determination should be based on an optimal balance between the cost required for the construction of this margin and the probability of pounding due to one or successive ground motions leading to a residual displacement of the structure on the same direction with the previous ground motion (Jampole et al. 2016).

The maxima of the acceleration response indicating the exceedance of the frictional resistance of the interface due to the subsequent excitations differ less than 10% from the values measured during the first excitation (Fig. 11). The presented stability of the frictional characteristics of the interface and the sliding behavior of the model structure for successive ground motion excitations confirm the repeatability of the beneficial effect of the proposed seismic isolation technique.

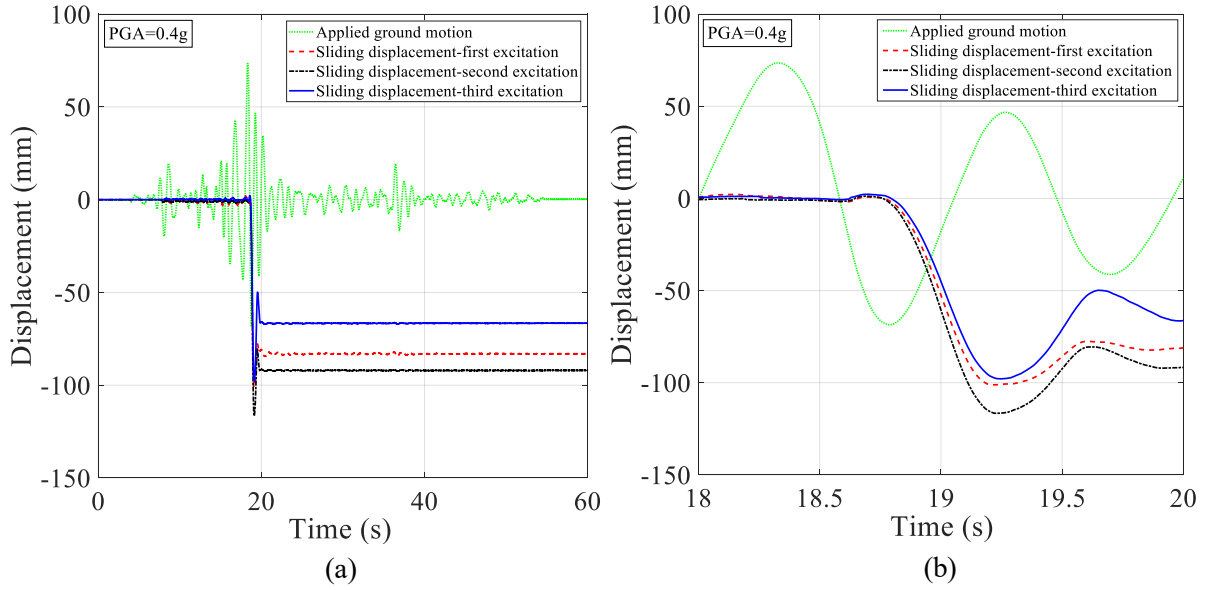


**Figure 10.** (a) Full and (b) magnified sliding displacement time history response of the concrete slab relative to the shaking table motion (mean value of CDX-SDX in Fig. 4) for three repetitions of the same Chi-Chi 1999 ground motion record (No. 1 in Table 2).

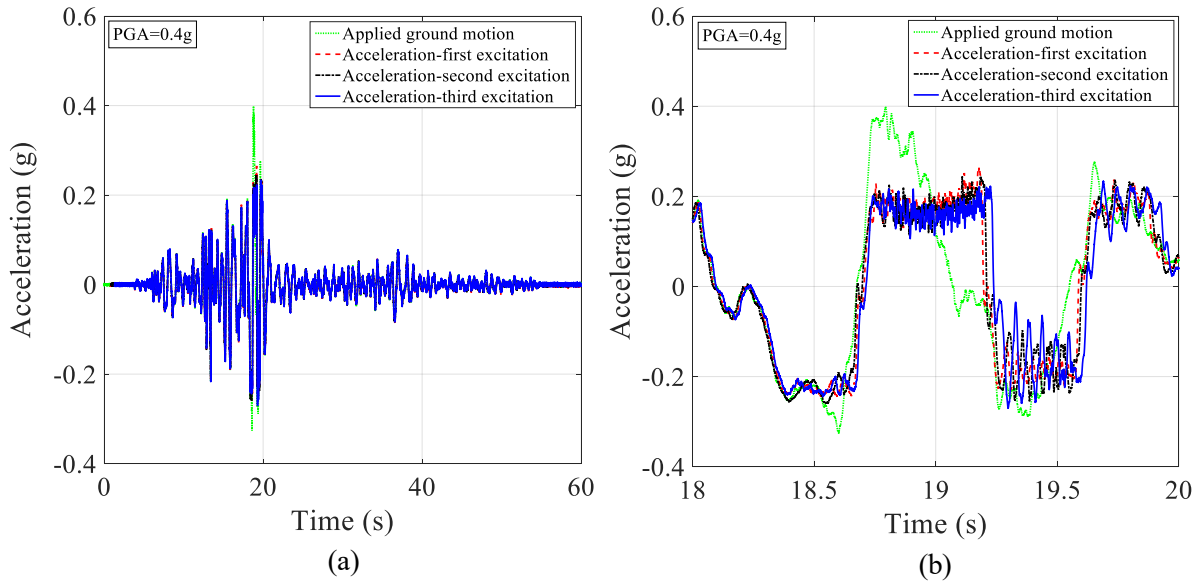


**Figure 11.** (a) Full and (b) magnified acceleration time history response of the concrete slab (mean value of C1X and C4X in Fig. 4) for three repetitions of the same Chi-Chi 1999 ground motion record (No. 1 in Table 2).

## SLIDING SYSTEM VERSUS FIXED-BASE STRUCTURE

The favorable effect of the proposed seismic isolation system is further highlighted through the comparison of the acceleration response of the seismically isolated steel structure with the response of the same structure, after the rigid attachment of its base to the shaking table (Fig.

12). The experimentally derived vibration period of the fixed-base structural system  $T_x=0.075s$  ( $f_x=13Hz$ ) is in good agreement with the design value of  $T_x=0.085s$  ( $f_x=12Hz$ ).

As shown in Fig. 13, the experimentally derived maximum acceleration of the seismically isolated structure subjected to Chi-Chi 1999 ground motion excitation (No. 1 in Table 2) is 2.5 times lower than the maximum acceleration of the fixed-base structure subjected to the same ground motion excitation. The reduction of the maximum seismic acceleration and the associated seismic force acting on the structure illustrates the efficiency of the proposed seismic isolation technique on the mitigation of seismic damage.



**Figure 12.** Experimental setup of the fixed-base structure.

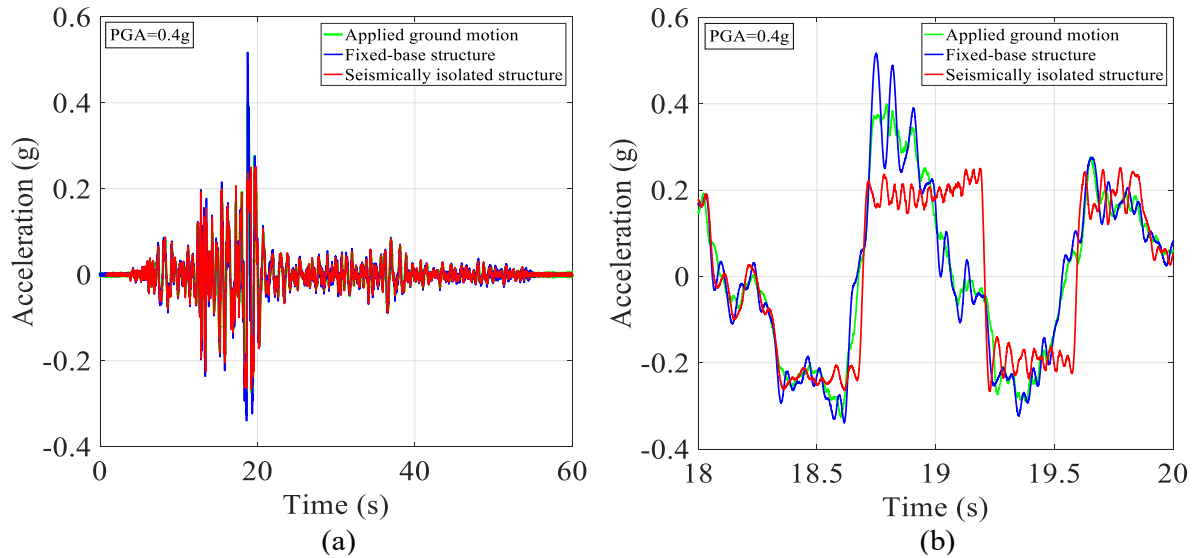


**Figure 13.** (a) Full and (b) magnified acceleration time history response of the steel structure (mean value of M1X and M4X in Fig. 4) subjected to Chi-Chi 1999 ground motion record (No. 1 in Table 2) for two configurations: 1) Fixed-base structure 2) Seismically isolated structure (PVC-s).

## INFLUENCE OF GROUND MOTION VARIATION

The influence of the variation of the ground motion characteristics on the efficiency of the proposed seismic isolation technique is quantified by subjecting the model structure to the

horizontal component of the Gorkha 2015 ground motion excitation (No. 3 in Table 2) and the Kobe 1995 ground motion excitation (No 7 in Table 2), scaled to the same  $PGA=0.4g$ . As shown Fig. 14 and 15, the maximum acceleration of the seismically isolated structure for the two ground motions is  $0.6g/0.3g=2$  and  $0.44g/0.28=1.57$  times lower than the corresponding fixed-base value.

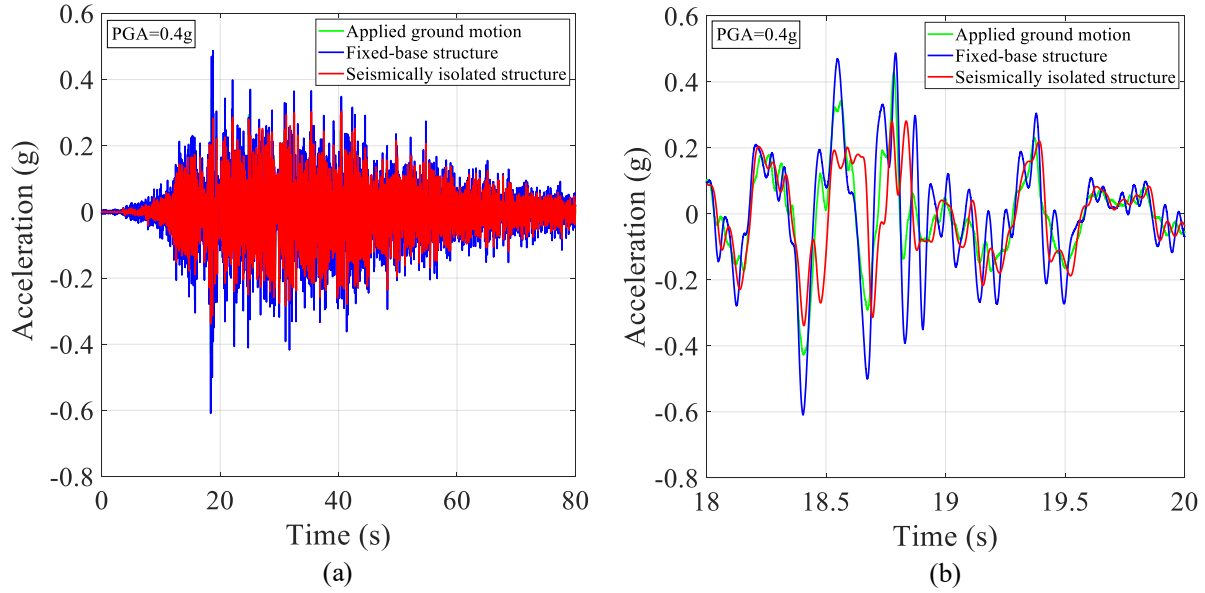


**Figure 14.** (a) Full and (b) magnified acceleration time history response of the steel structure (mean value of M1X and M4X in Fig. 4) subjected to Gorkha 2015 ground motion record (No. 3 in Table 2) for two configurations: 1) Fixed-base structure 2) Seismically isolated structure (PVC-s).

The hysteretic isolation force-sliding displacement response of the proposed PVC-s isolation system to Kobe 1995 ground motion excitation is shown in Fig. 15b. The corresponding force-displacement loop for the fixed-base superstructure subjected to the same ground motion excitation is also shown in the figure. The manifestation of no inelastic behavior and damage in the fixed-base superstructure subjected to a much higher force than the isolated case is attributed to its high stiffness and strength. This high strength is chosen due to the need for frequent crane transportation of the structure during the conduction of a large-scale experimental parametric investigation.

The values of the mean friction coefficient  $\hat{\mu}$ , the maximum acceleration of the isolated structure  $a_{isolated,max}$ , the maximum acceleration of the fixed-base structure  $a_{fixed-base,max}$ , the maximum sliding displacement  $u_{sliding,max}$ , the residual displacement  $u_{residual}$  and the maximum sliding velocity  $\dot{u}_{sliding,max}$  for all the ground motions considered in this study are summarized in Table 4 and Fig. 16. As shown in Table 4, the mean value of the reduction ratio between the



acceleration of the isolated structure and the acceleration of the fixed-base structure is 2.24. The high mean value of this ratio elucidates the efficiency of the proposed seismic isolation system for the ground motion ensemble presented in this study.

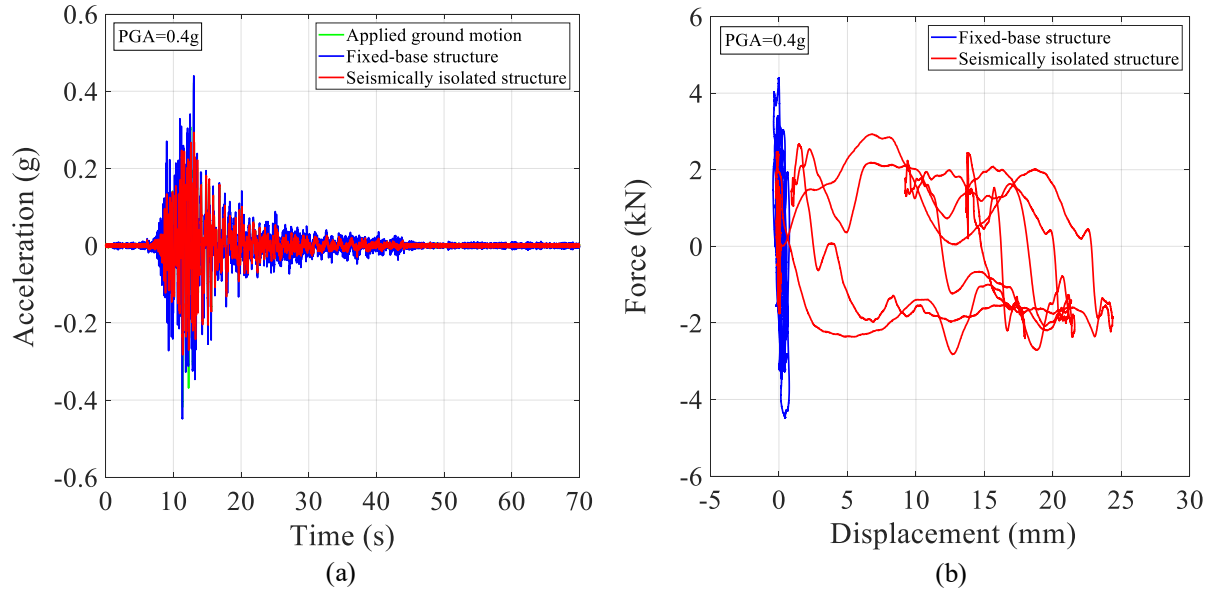


**Figure 15.** (a) Acceleration time history response and (b) hysteretic force-displacement loop of the structure subjected to Kobe 1995 ground motion record (No. 7 in Table 2) for two configurations: 1) Fixed-base structure 2) Seismically isolated structure (PVC-s).

**Table 4.** Mean and standard deviation values of the fundamental response parameters of the seismically isolated and the corresponding fixed-base structure due to the ground motions presented in this study (Ground motion ensemble shown in Table 2).

No.	PGA (g)	$\hat{\mu}$	$a_{isolated, max} (g)$	$a_{fixed-base, max} (g)$	$a_{isolated, max} / a_{fixed-base, max}$	$u_{sliding, max} (mm)$	$u_{residual} (mm)$	$\dot{u}_{sliding, max} (mm/s)$
1	0.4	0.187	0.25	0.52	2.08	100.64	83.31	373.4
2	0.6	0.162	0.35	0.81	2.31	145.78	11.88	650.7
3	0.4	0.211	0.30	0.61	2.03	9.47	6.99	90.5
4	0.6	0.194	0.37	0.92	2.49	57.21	43.04	261.9
5	0.4	0.202	0.33	0.63	1.90	8.79	5.69	92.8
6	0.6	0.162	0.35	1.01	2.89	67.25	39.83	636.1
7	0.4	0.192	0.28	0.44	1.57	23.67	12.95	245.7
8	0.6	0.179	0.37	0.70	1.89	76.34	20.52	395.8
9	0.5	0.190	0.30	0.90	3.0	100.08	99.11	333.4
$\hat{\mu}$		0.187	0.33	0.73	2.24	65.47	35.92	340.12
$\sigma$		0.015	0.04	0.18	0.45	43.68	32.31	190.04

The corresponding mean values for the maximum sliding displacement during each ground motion excitation  $u_{sliding, max}$  and residual displacement  $u_{residual}$  are 65.47mm and 35.92mm,

respectively. The mean value of the maximum sliding displacement indicates that the risk of pounding of the structure against the surrounding gravel and soil is minimal for the ground motion excitations investigated in this study. The low mean value of the residual displacement shows that the recentering of the prototype structure using pulling forces from trucks might be not required for many of the ground motions presented in this study (Fig. 16b) and the design of flexible pipe connections could protect the services (water, sewage system) of the structure from disruption.

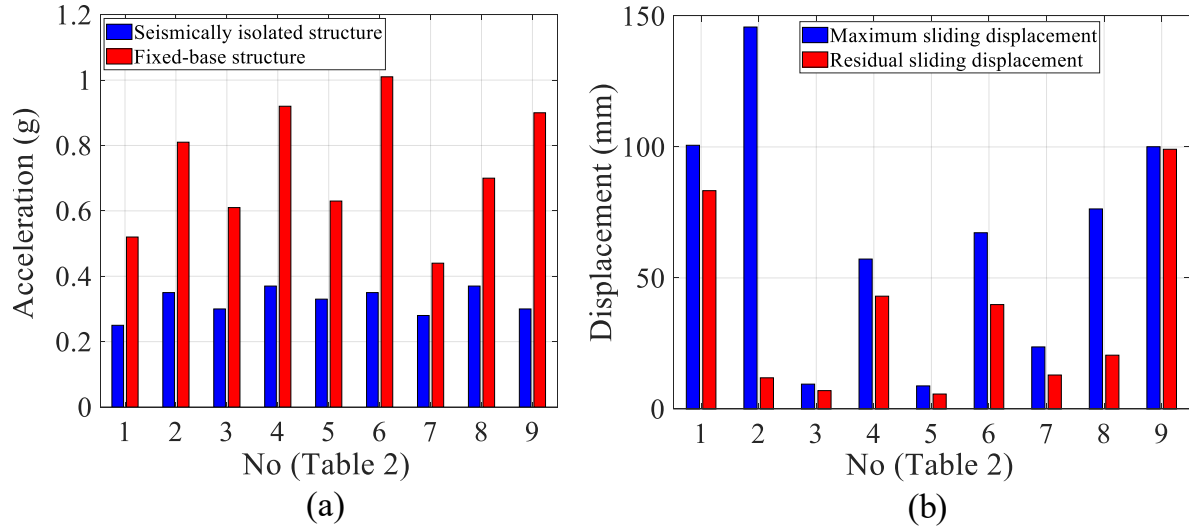


**Figure 16.** (a) Maximum acceleration and (b) Sliding displacement response of the model structure subjected to the earthquake records used in this study (Ground motion ensemble shown in Table 2).

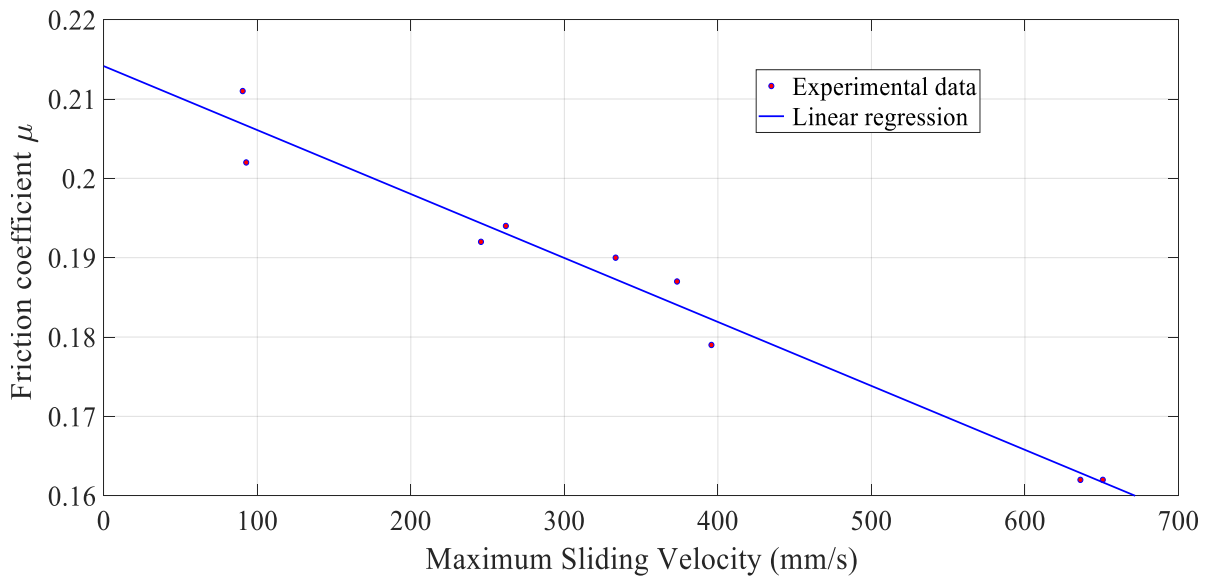


**Figure 17.** Friction coefficient  $\mu$  versus maximum sliding velocity of the model structure subjected to the earthquake records used in this study (Ground motion ensemble shown in Table 2).

As shown in Fig. 17, the decrease of the mean value of the friction coefficient for increased values of the maximum sliding velocity can be well approximated by a linear regression curve  $y=p_1x+p_2$  with  $p_1=-8.06 \cdot 10^{-5}$  and  $p_2=0.214$ . This linear decrease observed for maximum sliding velocity values above 90mm/s is consistent with the corresponding decrease of the friction coefficient value observed by Lomiento et al. (2013) for sliding bearings under seismic excitation.

#### INFLUENCE OF SIMULTANEITY OF GROUND MOTION COMPONENTS

The effect of the simultaneity of the three components of a ground motion excitation on the effectiveness of the presented PVC-s seismic isolation technique is determined through the investigation of the response of the model structure to L'Aquila 2009 ground motion excitation, scaled to a PGA=0.5g (No. 9 in Table 2). Furinghetti et al. (2017) highlighted the importance of the consideration of the biaxial interaction of the horizontal components of a ground motion excitation for the response of friction-based isolation systems due to the change in the orientation of the frictional force during the motion compared to the case of a unidirectional excitation. The destructive potential of vertical ground motion components during the L'Aquila 2009 earthquake has been presented by Verderame et al. (2011), Stewart et al. (2012) and Zimmaro et al. (2018).

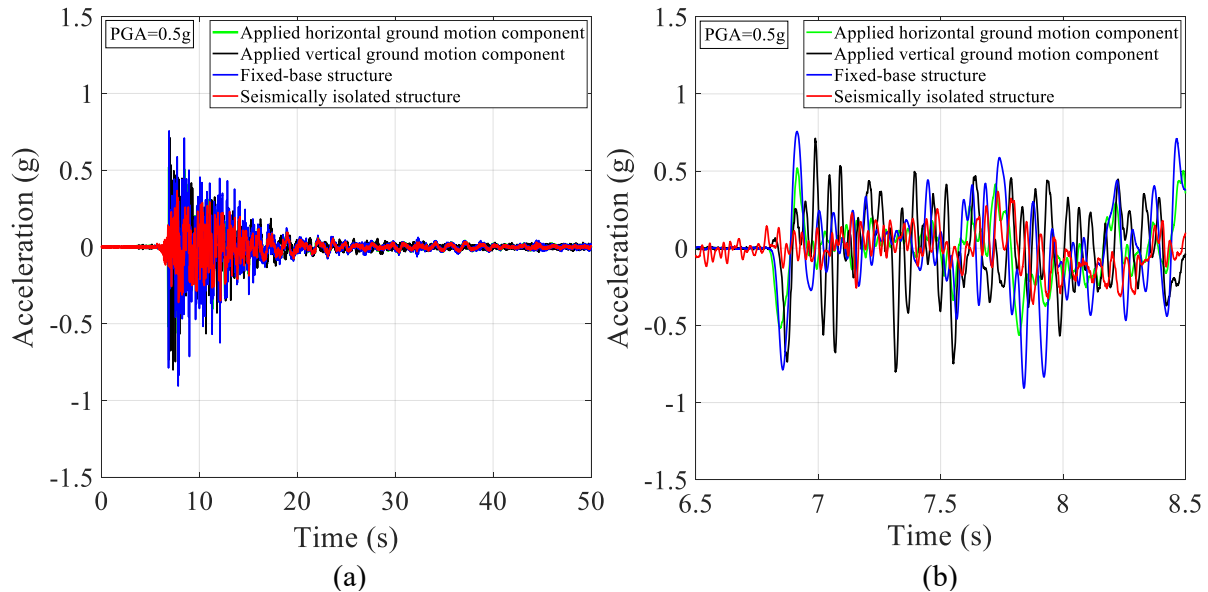


**Figure 18.** (a) Full and (b) magnified acceleration time history response of the steel structure (mean value of M1X and M4X in Fig. 4) subjected to L'Aquila 2009 ground motion record (No. 9 in Table 2) for two configurations: 1) Fixed-base structure 2) Seismically isolated structure (PVC-s).

The presence of a strong vertical ground motion component in the applied ground motion excitation did not inhibit the sliding behavior of the structure. As presented in Fig. 18, the acceleration reduction of the seismically isolated structure compared to the fixed-base case is  $0.9g/0.3g=3$ . The response of the structure subjected to this ground motion excitation indicates a possible independence of the performance of the presented seismic isolation from the presence of vertical ground motion components. However, the independence observed for this ground motion should be verified by future shaking table tests exciting the structure with an ensemble of records with strong vertical ground motion components. The potential effect of the phasing of these components on the performance of the proposed system could be also quantified by future experimental or analytical studies.

## **DESIGN REQUIREMENTS**

In light of the experimental results presented in this section, the proposed design requirements for the implementation of the proposed methodology in developing countries are:

- The presence of a flat ground surface (inclination  $<5^\circ$ ) as a base for the construction of the PVC-s configuration.
- The use of 6mm thick, upper and bottom PVC sheets for the sandwich configuration which cover at the minimum the dimensions of the foundation slab of the structure.
- The deposition of 750g of sand per  $m^2$  of the ‘sandwiched’ PVC area with a 20cm-height drop from the bottom PVC surface using a 2.2mm sieve.

## **EFFECT OF PVC SHEET DISCONTINUITIES**

The constructability of the presented seismic isolation technique in developing countries is a prerequisite for its wide application as a novel and practical design solution in these countries. Within this context, the investigation of the influence of an alternative PVC sheet configuration that entails the placement of two bottom  $2m \times 1.3m$  PVC sheets next to each other and below the concrete slab (Fig. 19) is interesting for two main reasons: first, it simulates a practical case, where multiple PVC sheets of smaller size are placed as the bottom sandwich surface of the prototype structure, as these PVC sheets are more economical and can be easily transported. Second, this configuration allows for the quantification of the effect of the discontinuity formed in the contact zone between the two PVC sheets on the sliding performance of the PVC-s seismic isolation technique. As shown in Fig. 20, the maximum acceleration response on the

concrete slab and the associated frictional characteristics of the PVC-sand-PVC interface are not significantly influenced by the presence of discontinuities in the bottom PVC sheet.

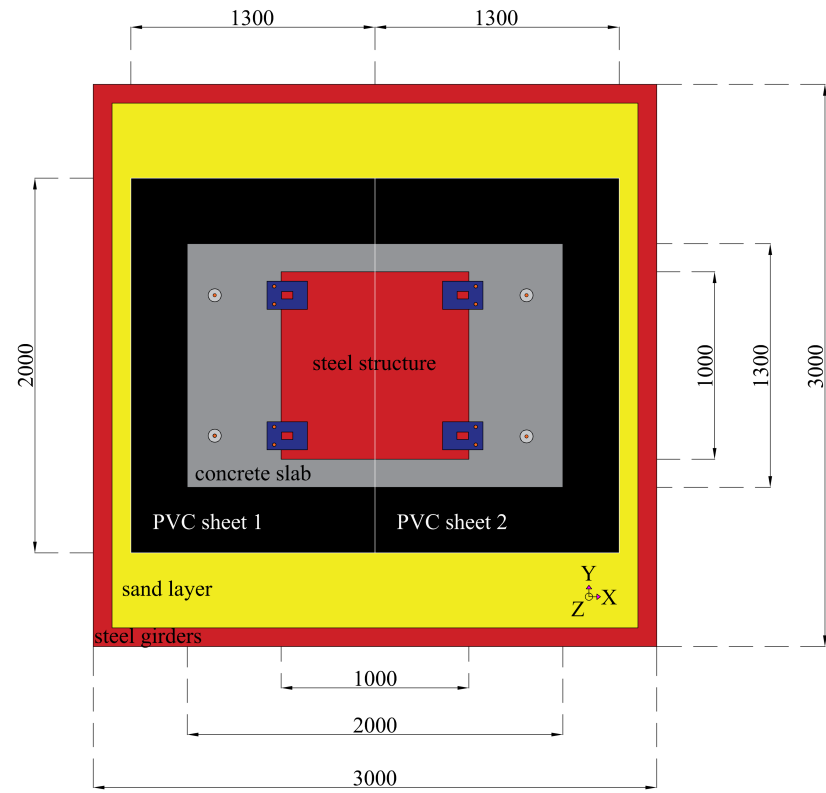


**Figure 19.** Overview of the configuration based on the use of two PVC sheets (Dimensions in mm).

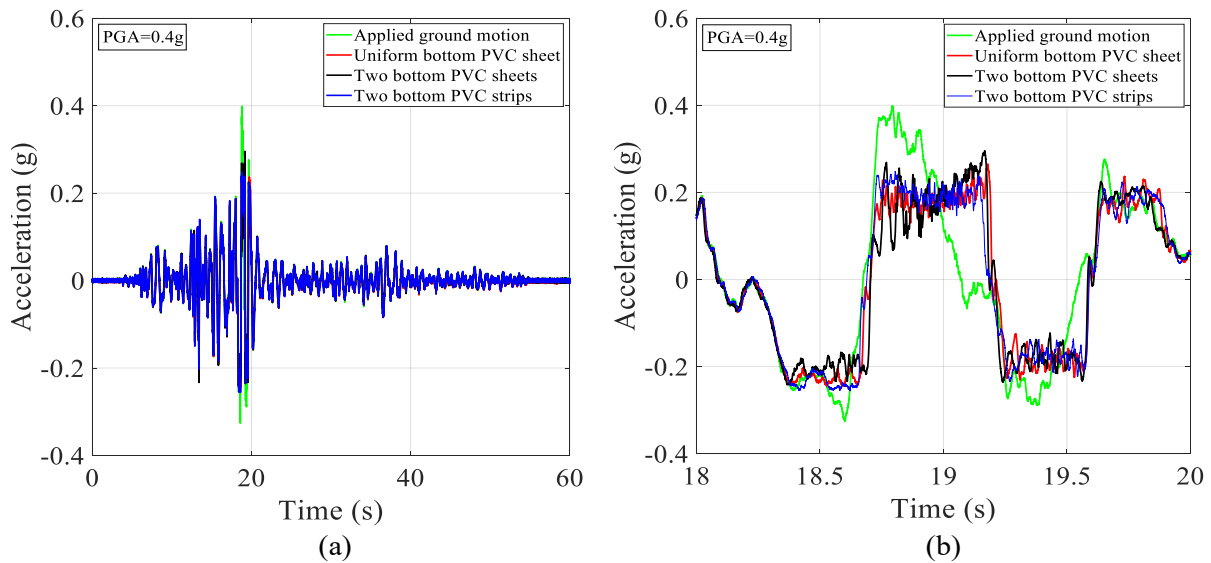


**Figure 20.** (a) Full and (b) magnified acceleration time history response of the concrete slab (mean value of C1X and C4X in Fig. 4) subjected to Chi-Chi 1999 ground motion record (No. 1 in Table 2) founded on two PVC sheets and comparison with the uniform PVC sheet configuration.

## IS THE WHOLE FOUNDATION SLAB NECESSARY?

The potential decrease of the contact surface between the PVC sheets and the concrete slab is investigated using two bottom 2mx0.2m PVC strips below the concrete slab, as shown in Fig. 21. This PVC configuration represents a case where the foundation slab of the prototype structure is replaced by four concrete foundation beams (strip footings), thus further reducing the construction cost of the proposed seismic isolation strategy.

The experimentally derived frictional behavior of the structure founded on the presented PVC strip interface (Fig. 21) does not substantially change compared to the original uniform PVC sheet configuration, as illustrated in Fig. 22. This independence of the performance of the proposed system from the bottom PVC configuration guarantees the constructability of the presented seismic isolation technique for various foundation slab geometries and indicates a potential construction cost decrease through the replacement of the concrete foundation slab by four concrete foundation beams.

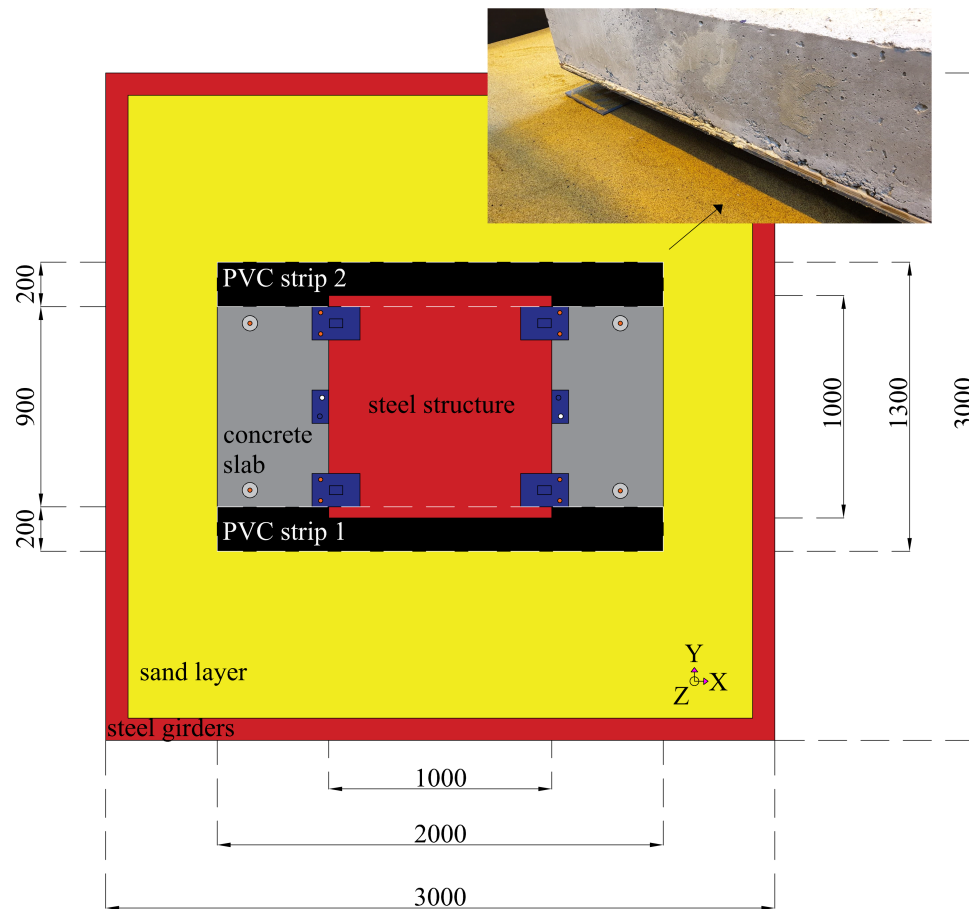


**Figure 21.** Overview of the configuration based on the use of two bottom PVC strips (Dimensions in mm).

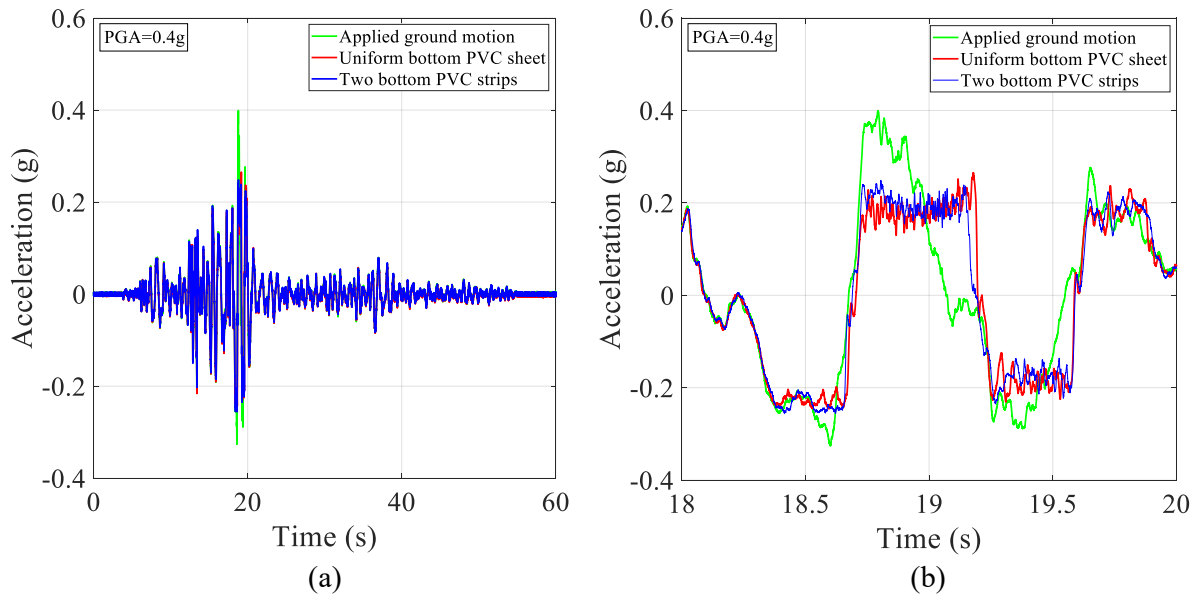


**Figure 22.** (a) Full and (b) magnified acceleration time history response of the concrete slab (mean value of C1X and C4X in Fig. 4) subjected to Chi-Chi 1999 ground motion record (No. 1 in Table 2) founded on two PVC strips and comparison with the uniform PVC sheet configuration.

## CONCLUSIONS

The large-scale experimental investigation presented in this study focuses on the effect of an innovative, low-cost PVC ‘sand-wich’ (PVC-s) seismic isolation system towards seismic damage mitigation in developing countries. The robustness of this seismic isolation strategy is attributed to the presence of two sliding mechanisms: The fundamental seismic protection mechanism, characterized by the relative sliding between two PVC sheets with encapsulated sand grains, is activated for ground motions of moderate earthquake intensity, corresponding roughly to a PGA of 0.25g. The optimal sand surface density range between 40 and 750g/m<sup>2</sup> that leads to the presented sliding behavior is experimentally determined. Within this density range, the sand surface density value of 750g/m<sup>2</sup> is recommended in this study as it renders the lowest dispersion of the friction coefficient. A secondary mechanism, triggered by the sliding behavior of a PVC surface against a sand foundation layer below the bottom PVC can be activated for ground motions of higher earthquake intensity, exceeding a PGA=0.35g.

The repeatability and the efficiency of the presented seismic isolation technique for subsequent ground motions of different characteristics and alternative PVC sheet configurations is experimentally validated. The beneficial effect of the PVC-s seismic isolation strategy on the reduction of seismic accelerations and forces is shown through a comparison with the experimentally derived response of the corresponding fixed-base structure.

The activation of the sliding behavior of the structure using the proposed seismic isolation for a ground motion containing a strong vertical component is presented. Nevertheless, the conduction of future large-scale tests exploring the performance of the proposed system for a wide range of ground motion records with vertical components is required for the generalization of the trends observed for this ground motion. The frictional characteristics of the proposed interface are also found to be preserved even for the case of a placement of the bottom PVC layer in two separate pieces, which shows the constructability of the proposed seismic isolation technique in countries with transportation of PVC availability issues. A reduction of the bottom PVC surface using PVC strips yielded equivalent results with the case of a uniform bottom PVC sheet, thus indicating a potential, more economical replacement of the bottom concrete slab by four concrete beams (strip footings) based on PVC strips.

The presence of residual horizontal displacements of a maximum amplitude of 10cm and a mean amplitude of 3.6cm is expected after the occurrence of strong ground motion excitations. However, the low amplitude of these expected displacement estimates allows for a relatively simple recentering of the displaced low-rise structure using pulling forces from trucks or other types of vehicles.

Inevitably, there are some inherent limitations in the findings derived from the large-scale investigation presented in this study. First, the sliding response observed for the geometry of the selected test structure simulating a typical masonry school located in Nepal should be generalized to other geometries by future experimental studies. Second, the experimentally convenient choice of a steel test structure of higher strength compared to an alternative masonry test structure cannot shed light on the seismic damage of a fixed-base masonry structure. Therefore, the efficiency of the holistic hybrid design approach presented in this study will be further verified by a large-scale shaking table investigation of a scaled-down masonry model of the prototype structure at the shaking table of University of Bristol.

## ACKNOWLEDGEMENTS

This work is supported by the EPSRC-funded research project ‘SAFER’ (Seismic Safety and Resilience of Schools in Nepal, EP/P028926/1). Prof. George Mylonakis is gratefully acknowledged for his input on the dimensional analysis performed in this study. The authors would like to thank Dr. Adam Crewe for his recommendations on the design of the experimental setup. The technicians Mr. Dave Ward, Mr. Mitchell Mictroy, the postdoctoral researcher Dr. Nicola Giordano and the students Mr. Giorgos Lamprakis, Mr. Ioannis



Koromilas, Mr. Felipe Vicencio, Mr. Francesco Di Michele and Dr. Nikolaos Psyrras are kindly acknowledged for their technical assistance in the presented shaking table tests.

## REFERENCES

- Bowden, F.P., and Tabor, D., 1956. The Friction and Lubrication of Solids. Clarendon Press, Oxford, 372 pp.
- Buckle, I.G., and Mayes, R.L., 1990. Seismic isolation history, application and performance—a world view, *Earthquake Spectra* **6** (2), 161–201.
- Calantariens, J.A., 1909. Improvements in and Connected with Building and Other Works and Appurtenances to Resist the Action of Earthquakes and the Like, Paper No. 325371, Engineering Library, Stanford University, Stanford, California.
- Cilsalar, H., and Constantinou, M.C., 2019. Behavior of a spherical deformable rolling seismic isolator for lightweight residential construction, *Bulletin of Earthquake Engineering* **17** (7), 4321-4345.
- Constantinou, M.C., Kartoum, A., Reinhorn, A.M., and Bradford, P., 1992. Sliding isolation system for bridges: Experimental study, *Earthquake Spectra* **8**, 321-344.
- Coulomb, C.A., 1785. Theorie des machines simples, en ayant egard au frottement de leur parties st a la roideur des cordages, *Memorie de Mathematique et de Physique de l'Academie Royale* **10**, 161-332.
- Dove, J. E., and Frost, J. D., 1999. Peak friction behavior of smooth geomembrane-particle interfaces, *Journal of Geotechnical and Geoenvironmental Engineering ASCE* **125** (7), 544–555.
- Dupuit, A.J.E.J., 1842. Memoire sur le triage des voitures et sur le frottement du roulement, *Annales des ponts et chausees* **3**, 261-335.
- Ebrahimian, B., Noorzad, A., and Alsaleh, M.I., 2019. A numerical study on interface shearing of granular Cosserat materials, *European Journal of Environmental and Civil Engineering*, DOI: 10.1080/19648189.2019.1627249.
- Furinghetti, M., and Pavese, A., 2017. Equivalent Uniaxial Accelerogram for CSS-Based Isolation Systems Assessment under Two-Components Seismic Events, *Mechanics Based Design of Structures and Machines*, DOI: 10.1080/15397734.2017.1281145.
- Furinghetti, M., Pavese, A., Quaglini, V., and Dubini, P., 2019a. Experimental Investigation of the cyclic response of double curved surface sliders subjected to radial and bidirectional sliding Motions, *Soil Dynamics and Earthquake Engineering*, DOI: 10.1016/j.soildyn.2018.11.020
- Furinghetti, M., Casarotti, C., and Pavese, A, 2019b. Investigation of the consequences of mounting laying defects for curved surface slider devices under general seismic input, *Journal of Earthquake Engineering* **23**(3), 377-403, DOI: 10.1080/13632469.2017.1323046.

620 Heaton, T. H., Hall, J. F., Wald, D. J., and Halling, M. W., 1995. Response of high-rise and base-  
621 isolated buildings to a hypothetical Mw 7.0 blind thrust earthquake, *Science* **267** (13), 206–211

622 Jampole, E., Deierlein, G., Miranda, E., Fell, B., Swensen, S., and Acevedo, C., 2016. Full-scale  
623 dynamic testing of sliding seismically isolated unibody house, *Earthquake Spectra* **32** (4), 2245–  
624 2270.

625 Kelly, J.M., 1990. Base Isolation: Linear Theory and Design, *Earthquake Spectra* **6** (2), 223-244.

626 Kelly, J.M., 2002. Seismic isolation systems for developing countries, *Earthquake Spectra* **18**, 385–  
627 406.

628 Kumar, M., Whittaker, A.S. and Constantinou, M.C., 2015. Characterizing friction in sliding isolation  
629 bearings, *Earthquake Engineering and Structural Dynamics* **44**, 1409–1425.

630 Li, Z., Rossow, E.C., and Shah, S.P., 1989. Sinusoidal forced vibration of sliding masonry system,  
631 *Journal of Structural Engineering ASCE* **115**, 1741–55.

632 Lomiento, G., Bonessio, N., and Benzoni, G., 2013. Friction model for sliding bearings under seismic  
633 excitation. *Journal of Earthquake Engineering* **17**(8), 1162–1191.

634 Miranda, E. and Bertero, V., 1994. Evaluation of strength reduction factors of earthquake-resistant  
635 design, *Earthquake spectra* **10** (2), 357-379.

636 Mylonakis, G., and Gazetas, G., 2000. Seismic soil-structure interaction: beneficial or detrimental?  
637 *Journal of Earthquake Engineering* **4** (3), 277–301.

638 Naeim, F., 2019. Performance-based seismic design of tall buildings—A USA perspective, In:  
639 Kasimzade A., Şafak E., Ventura C., Naeim F., Mukai Y. (eds): Seismic isolation, structural health  
640 monitoring, and performance based seismic design in earthquake engineering, Springer, Cham.

641 Naeim, F., and Kelly, J. M., 1999. Design of Seismic Isolated Structures—From Theory to Practice,  
642 John Wiley and Sons, New York.

643 Nanda, R.P., Shrikhande, M., and Agarwal, P., 2016. Low-cost base-isolation system for seismic  
644 protection of rural buildings, *ASCE Practice Periodical of Structural Design and Construction* **21**  
645 (1), 04015001.

646 O’Rourke, T.D., Druschel, S.J., and Netravali, A.N., 1990. Shear strength characteristics of sand-  
647 polymer interfaces, *Journal of Geotechnical Engineering ASCE* **116** (3), 451–469.

648 Pavese, A., Furinghetti, M., and Casarotti, C., 2019. Investigation of the consequences of mounting  
649 laying defects for curved surface slider devices under general seismic input, *Journal of Earthquake*  
650 *Engineering*, DOI: 10.1080/13632469.2017.1323046.

651 PEER NGA Strong Motion Database, 2018. Pacific Earthquake Engineering Research Center,  
652 University of California, Berkeley, available at <https://ngawest2.berkeley.edu/> (last accessed 08  
653 October 2018).

654 Quaglini, V., Gandelli, E., and Dubini, P., 2019. Numerical investigation of Curved Surface Sliders  
655 under bidirectional orbits, *Ingegneria Sismica*, **36**(2), 118-136.

656 Shooter, K. V., and Tabor, D., 1952. The frictional properties of plastics, *Proceedings of the Physical*  
657 *Society* **65**, 661–671.

658 Star, L. M., Tileylioglu, S., Givens, M. J., Mylonakis, G., and Stewart, J. P., 2019. Evaluation of soil-  
659 structure interaction effects from system identification of structures subject to forced vibration tests,  
660 *Soil Dynamics and Earthquake Engineering* **116**, 747–760.

661 Stewart, J. P., and Fenves, G. L., 1998. System identification for evaluating soil–structure interaction  
662 effects in buildings from strong motion recordings, *Earthquake Engineering and Structural*  
663 *Dynamics* **27**, 869–885.

664 Stewart, J. P., Lanzo, G., Pagliaroli, A., Scasserra, G., Di Capua, G., Peppoloni, S., Darragh, R. B., and  
665 158 Gregor, M., 2012. Ground Motion Recordings from the Mw 6.3 2009 L’Aquila Earthquake in  
666 Italy 159 and their Engineering Implications, *Earthquake Spectra* **28**, 317-345.

667 Taciroglu, E., Çelebi, M., Ghahari, S. F., and Abazarsa, F., 2016. An investigation of soil-structure  
668 interaction effects observed at the MIT Green Building, *Earthquake Spectra* **32** (4), 2425–2448.

669 Tsang, H.H., and Pitilakis, K., 2019. Mechanism of Geotechnical Seismic Isolation System: Analytical  
670 Modeling, *Soil Dynamics and Earthquake Engineering* **122**, 171-184.

671 Tsiavos, A., Alexander, N., Diambra, A., Ibraim, E., Vardanega, P., Gonzalez-Buelga, A., and Sextos,  
672 A., 2019. A sand-rubber deformable granular layer as a low-cost seismic isolation strategy in  
673 developing countries: experimental investigation, *Soil Dynamics and Earthquake Engineering* **125**,  
674 October 2019, 105731, DOI: <https://doi.org/10.1016/j.soildyn.2019.105731>.

675 USGS Center for Engineering Strong Motion Data, available at <https://strongmotioncenter.org/> (last 08  
676 October 2018).

677 Verderame, G.M., De Luca, F., Ricci, P., and Manfredi, G., 2011. Preliminary analysis of a soft-storey  
678 mechanism after the 2009 L’Aquila earthquake, *Earthquake Engineering and Structural Dynamics*  
679 **40** (8), 925–44.

680 Wilding, B.V., and Beyer, K., 2018. The effective stiffness of modern unreinforced masonry walls,  
681 *Earthquake Engineering and Structural Dynamics* **47**, 1683–1705.

682 Wright, F. L., 1977. An Autobiography: Frank Lloyd Wright, Horizon Press, New York.

683 Yang, T.Y., Konstantinidis, D., and Kelly, J.M., 2010. The influence of isolator hysteresis on equipment  
684 performance in seismic isolated buildings, *Earthquake Spectra* **26** (1), 275-293.

685 Zimmaro, P., Scasserra, G., Stewart, J. P., Kishida, T., Tropeano, G., Castiglia, M., and Pelekis, P.,  
686 2018. Strong ground motion characteristics from 2016 Central Italy earthquake sequence,  
687 *Earthquake Spectra* **34** (4), 1639-1669.